ARCHITECTURAL RESEARCH, Vol. 7, NO. 1 (2005), pp. 27-38

The Bearing Strength of Connections Between Steel Coupling Beam and Reinforced Concrete Shear Walls

Hyun Do Yun, Wan Shin Park, Min Ki Han, Sun Woo Kim
Department of Architectural Engineering, Chungnam National University, Daejon, Korea
Yong Chul Kim and Sun Kyung Hwang
Dong-Yang Structural Engineering, Daejon, Korea
Department of Architecture, Woosong University, Daejon, Korea

Abstract

No specific guidelines are available for computing the bearing strength of connection between steel coupling beam and reinforced concrete shear wall in a hybrid wall system. There were carried out analytical and experimental studies on connection between steel coupling beam and concrete shear wall in a hybrid wall system. The bearing stress at failure in the concrete below the embedded steel coupling beam section is related to the concrete compressive strength and the ratio of the width of the embedded steel coupling beam section to the thickness of the shear walls. Experiments were carried out to determine the factors influencing the bearing strength of the connection between steel coupling beam and reinforced concrete shear wall. The test variables included the reinforcement details that confer a ductile behavior in connection between steel coupling beam and shear wall, *i.e.*, the auxiliary stud bolts attached to the steel beam flanges and the transverse ties at the top and the bottom steel beam flanges. In addition, additional test were conducted to verify the strength equations of the connection between steel coupling beam and reinforced concrete shear wall. The proposed equations in this study were in good agreement with both our test results and other test data from the literature.

Keywords: Steel coupling beams, Bearing strength, Connection

1. INTRODUCTION

Properly designed coupled walls have many desirable earthquake-resistant design features. Large lateral stiffness and strength can be achieved. By coupling beam individual flexural walls, the lateral load resisting behavior changes to on where overturning moments are resisted partially by an axial compression-tension couple across the wall system rather than by the individual flexural action of the walls. The beams that connect individual wall piers are referred to as coupling beams. In order for the desired behavior of the hybrid wall system to be attained, the coupling beams, however, must also yield before the wall piers, behave in a ductile manner, and exhibit significant energy absorbing characteristics. Several researchers have investigated novel approaches to improve the ductility and energy absorption of reinforced concrete coupling beams. Specially detailed diagonal reinforcement was developed by Pauley and Binney [1] for span-to depth ratios below a value of about two, and these significantly improve the reversed cyclic loading response. In this form of construction, closely spaced hoops or spiral reinforcement confining the diagonal bars, both in the coupling beam and along their wall embedment, are required. Shiu *et al*. [2] have confirmed the improved behavior of diagonally reinforced beams over conventional reinforced beam designs. However, these tests demonstrated that for larger span-to-depth ratios (values of 2.5 and 5), diagonal reinforcement was not as efficient due to its lower inclination, and therefore, lower contribution to the shear resistance.

Steel link beams serve as the primary energy-absorbing elements in eccentrically braced frames: a role similar to that played by reinforced concrete coupling beams in coupled wall systems. Roader and Popov [3] have shown that steel link beams in eccentrically braced frames can be detailed to provide excellent ductility and energy dissipating characteristics. In addition, Gong *et al*. [4] have shown that stiffeners are not required for a composite coupling beam.

As mentioned above, a number of recent studies have focused on examining the seismic response of concrete, steel, and composite coupling beams. However, since no specific equations are available for computing the bearing strength of connection between steel coupling beam and reinforced concrete shear wall, it is necessary to develop such strength equations. In this study, it were set out to develop the strength equations of connection between steel coupling beam and reinforced concrete shear wall in a hybrid wall system, and analytical and experimental studies on joint of steel coupling beam-concrete shear wall were carried out. A flow chart of the main research topics is shown in Fig. 1. Six two-third-scale subassemblies were designed, constructed, and tested. Each specimen consisted of a wall pier and a steel beam embedded in the wall to represent a steel coupling beam, and the test results are discussed later on. Governed by the bearing on the concrete, the experimental results of specimens subjected to reverse cyclical loading were used to revise and verify the proposed strength equation capacities of connection between steel coupling beam and reinforced concrete shear wall.

2. ANALYTICAL STUDY

2.1 Bearing strength of concrete above and below the embedded steel section

Since the coupling beam is expected to undergo significant inelastic deformation, then its embedment must be capable of developing forces corresponding to the plastic capacity of the beam. No specific guidelines are available for computing the bearing strength of connection between

steel coupling beam and reinforced concrete shear wall, but references to previous studies show the adequacy of four models proposed by the Prestressed Concrete Institute (PCI), Chicago, USA [5, 6], Kriz and Raths [7], Williams [8], and Mattock and Gaafar [9]. These four models were originally developed for the design of precast, bracket, corbel, and beam-column joint, respectively, and have been used to propose equations describing the strength of connection between steel coupling beam and reinforced concrete shear wall.

Figure 2 shows actual and assumed stresses and strains for connection between steel coupling beam and reinforced concrete shear wall. The compressive stresses in the concrete above and below the embedded steel section caused by the load, V_n, acting on the section at a given distance from the face of the concrete shear walls are shown in Fig. 2(a). The applied shear (V_n) is resisted by mobilizing an internal moment arm between the bearing forces, C_f and C_b. For calculation purposes, the stresses in the concrete at the ultimate stress are assumed to be as shown in Fig. 2(b). The parabolic compressive stress distribution below the embedded steel coupling beam section has been replaced by the equivalent rectangular stress distribution, equal to $0.85f_{ck}$, which is defined in Section 10.2.7 of the ACI 318-02 report [14].

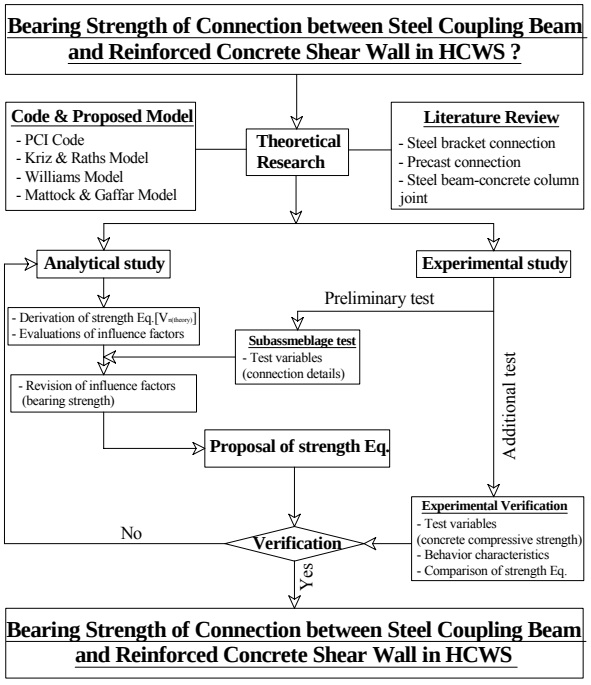

Fig. 1 Flow chart of the main research topic

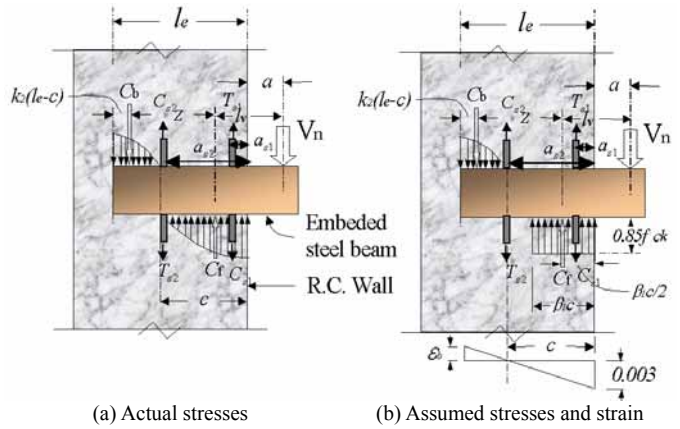

(a) Actual stresses (b) Assumed stresses and strain

Fig. 2 Actual and assumed stresses and strains in concrete adjacent to embedded steel coupling beam section

The parabolic distribution of bearing stresses above the embedded steel coupling beam section is assumed to obey the following stress-strain relationship proposed by Kent and Park [15]

$$f_c = f_{ck}\left[\frac{2\varepsilon_c}{0.002} - \left(\frac{\varepsilon_c}{0.002}\right)^2\right] \text{ (MPa)} \tag{1}$$

and is also assumed that there is a linear relationship between the compressive strains above and below the steel coupling beam section, as shown in Fig. 2(b). The assumed stress-strain relationship for concrete above the embedded steel coupling beam section corresponds to a parabola with a maximum stress of f_{cu} at a strain = 0.002. The factor, k_2, defining the location of the resultant compressive force, C_b, is given by

$$k_2 = 1 - \frac{\int_0^{\varepsilon_{cm}} \varepsilon_b f_c d\varepsilon}{\varepsilon_{cm}\int_0^{\varepsilon_{cm}} f_c d\varepsilon} = 1 - \frac{\int_0^{\varepsilon_{cm}} \{\varepsilon_b \times 1{,}000\, f_{ck}(\varepsilon - 250\varepsilon^2)d\varepsilon\}}{\varepsilon_{cm}\int_0^{\varepsilon_{cm}} \{1{,}000\, f_{ck}(\varepsilon - 250\varepsilon^2)d\varepsilon\}}$$
$$= \left[\frac{1-125\varepsilon_b}{3-500\varepsilon_b}\right] \tag{2}$$

and the resultant compressive force, C_b, is given by

$$C_b = \alpha f_{ck} bkd = \left[\frac{\int_0^{\varepsilon_{cm}} f_c d\varepsilon}{f_{ck}\varepsilon_{cm}}\right] \times f_{ck} bkd$$
$$= \frac{500}{3} f_{ck}\left[3\varepsilon_b - 500\varepsilon_b^2\right](l_e - c)b$$

where, $\alpha = \dfrac{\int_0^{\varepsilon_{cm}} f_c d\varepsilon}{f_{ck}\varepsilon_{cm}}$

As

$$\varepsilon_b = 0.003\,(l_e - c)/c$$

therefore

$$C_b = 0.5\frac{b}{c} f_{ck}(l_e - c)^2\left[3 - 1.5\left(\frac{l_e - c}{c}\right)\right] \tag{3}$$

and

$$k_2 = \left[\frac{1 - 0.375\left(\dfrac{l_e - c}{c}\right)}{3 - 1.50\left(\dfrac{l_e - c}{c}\right)}\right] \tag{4}$$

Using the equivalent rectangular stress distribution, the resultant compressive force, C_f, is given by

$$C_f = 0.85\, f_{ck}\beta_1 cb \tag{5}$$

Taking moments about the centre of action of V_n gives

$$C_f l_v = C_b(l_v + Z) \tag{6}$$

$$l_v = (a + \beta_1 c/2) \tag{7}$$

and

$$(l_v + Z) = a + l_e - k_2(l_e - c) \tag{8}$$

Substituting for C_b, C_f, l_v, and (l_v+Z) in Equation (8) gives

$$0.85\, f_{ck}\beta_1 cb\left(a+\beta_1 c/2\right)=0.5\frac{b}{c}f_{ck}\left(l_e-c\right)^2\left[3+1.5\left(\frac{l_e-c}{c}\right)\right]\times\left\{a+l_e-\left(l_e-c\right)\left[\frac{1-0.357\left(\frac{l_e-c}{c}\right)}{3-1.50\left(\frac{l_e-c}{c}\right)}\right]\right\}$$

Transposing yields

$$1.7\beta_1\left(\frac{c}{l_e}\right)^2\left[\frac{a}{l_e}+\beta_1\left(\frac{c}{l_e}\right)\right]-\left(\frac{c}{l_e}+1\right)^2\left[\left(\frac{a}{l_e}+1\right)\left(4.5-1.5\frac{l_e}{c}\right)-\left(1-\frac{c}{l_e}\right)\left(1.375-0.375\frac{l_e}{c}\right)\right]=0 \quad (9)$$

The distance c may be obtained from Equation (9) for

Table 1. Comparison with other test data

Researcher	Specimen Name	b (mm)	b_{eff} (mm)	c (mm)	l (mm)	l_e (mm)	l_v (mm)	l_{eff} (mm)	t (mm)	a (mm)	f_{cu} (MPa)	b/t (-)	e (mm)	Section (mm)	$V_{n(test)}$ (kN)
Mattock & Gaafar[5] (1982)	R2	50.8	-	38.1	-	254	-	-	254	102	27.8	0.20	-	4.45×2	247.0
	R5	127.0	-	38.1	-	254	-	-	254	102	28.3	0.50	-	3.24×5	340.1
	I3	76.2	-	38.1	-	254	-	-	254	102	26.6	0.30	-	H-101×76×25×25	298.2
	I3F	76.2	-	38.1	-	254	-	-	254	102	27.5	0.30	-	H-101×76×25×25	233.6
	W4	101.6	-	38.1	-	203	-	-	254	152	20.3	0.40	-	H-152×101×58×71	169.1
Clarke & Symmons[6] (1978)	B1(3)	38	-	40	-	125	150	-	145	50	33.0	0.26	-	38×38	90.0
	B2(1)	51	-	40	-	125	150	-	150	50	23.2	0.34	-	51×51	85.0
	B2(2)	51	-	40	-	125	150	-	150	50	23.2	0.34	-	51×51	80.0
	B2(3)	51	-	40	-	125	150	-	150	50	16.6	0.34	-	51×51	56.0
	B3(1)	51	-	40	-	125	150	-	150	50	20.9	0.34	-	51×38	62.0
	B3(2)	51	-	40	-	125	150	-	150	50	20.9	0.34	-	51×38	60.0
	B3(3)	51	-	40	-	125	150	-	150	50	20.9	0.34	-	51×38	67.0
	B4(1)	76	-	40	-	125	150	-	150	50	23.2	0.51	-	76×51	91.0
	B4(2)	76	-	40	-	125	150	-	150	50	16.6	0.51	-	76×51	80.0
	B4(3)	76	-	40	-	125	150	-	150	50	16.6	0.51	-	76×51	70.0
	C2(1)	51	-	40	-	125	150	-	150	50	16.6	0.34	-	51×51	66.0
	C2(2)	51	-	40	-	125	150	-	150	50	16.6	0.34	-	51×51	68.0
	C2(3)	51	-	40	-	125	150	-	150	50	16.6	0.34	-	51×51	77.0
	C3(1)	51	-	40	-	125	150	-	149	50	29.0	0.34	-	51×38	90.0
	C3(2)	51	-	40	-	125	150	-	149	50	29.0	0.34	-	51×38	90.0
	C3(3)	51	-	40	-	125	150	-	149	50	29.0	0.34	-	51×38	90.0
	C4(1)	76	-	40	-	125	150	-	150	50	20.8	0.51	-	76×51	92.0
	C4(2)	76	-	40	-	125	150	-	150	50	16.6	0.51	-	76×51	72.0
	C4(3)	76	-	40	-	125	150	-	147	50	30.6	0.52	-	76×51	124.0
	D1(1)	38	-	40	-	125	150	-	150	50	26.5	0.25	-	38×38	80.0
	D1(2)	38	-	40	-	125	150	-	150	50	26.5	0.25	-	38×38	80.0
	D1(3)	38	-	40	-	125	150	-	150	50	26.5	0.25	-	38×38	80.0
	D2(1)	51	-	40	-	125	150	-	150	50	20.8	0.34	-	51×51	84.0
	D2(2)	51	-	40	-	125	150	-	150	50	16.6	0.34	-	51×51	71.0
	D2(3)	51	-	40	-	125	150	-	150	50	16.6	0.34	-	51×52	74.0
	D3(1)	51	-	40	-	125	150	-	150	50	21.6	0.34	-	51×38	93.0
	D3(2)	51	-	40	-	125	150	-	150	50	21.6	0.34	-	51×38	97.0
	D3(3)	51	-	40	-	125	150	-	150	50	21.6	0.34	-	51×38	94.0
	D4(1)	76	-	40	-	125	150	-	150	50	26.6	0.51	-	76×51	130.0
Marcakis & Mitchell[7] (1980)	C1	101.6	-	40	-	152	-	-	178	76	33.1	0.57	-	4×4×1/4 tube*	123.7
	C2	101.6	-	40	-	152	-	-	178	76	26.9	0.57	-	4×4×1/4 tube#	184.2
	C3	101.6	-	40	-	152	-	-	178	76	35.9	0.57	-	4×4×1/4 tube#	200.2
	C4	101.6	-	40	-	152	-	-	178	76	40.0	0.57	-	4×4×1/4 tube#	238.0
	SC2	101.6	-	40	-	178	-	-	203	76	31.0	0.50	-	6×4×3/2 tube#	244.7
	SC3	101.6	-	40	-	178	-	-	203	102	31.0	0.50	-	6×4×3/2 tube#	314.5
	SC4	101.6	-	40	-	178	-	-	203	102	31.0	0.50	-	6×4×3/2 tube#	297.1
	SC5	101.6	-	40	-	178	-	-	203	102	31.0	0.50	-	6×4×3/2 tube#	244.7
	SC6	101.6	-	40	-	178	-	-	203	102	31.0	0.50	-	W6in×25Ib$	270.9
	SC9	101.6	-	40	-	178	-	-	184	111	31.0	0.55	-	6×4×3/8 tube#	218.4
	SC10	101.6	-	40	-	194	-	-	254	76	31.0	0.40	-	6×4×3/8 tube#	279.3
	TC1	101.6	-	40	-	184	-	-	406	102	23.4	0.25	-	4×4 solid bar	262.0
	PL1	19.05	-	40	-	102	-	-	203	76	47.6	0.09	-	3/4×4 plate	87.2
Bahram M. Shahrooz[8] (1993)	W1	203.0	254.0	40.0	434.0	229	-	189	254	267	35.0	0.80	352	H-457×203×25×25	246.9
Kent Harries[9] (1995)	S1	135.0	200.0	40.0	1200.0	600	-	560	300	600	25.9	0.45	920	H-347×135×5×19	303.0

* Tube empty
\# Tube filled with concrete
$ Flanges cut to 4in. wide

any particular combination of a, l_e, and β_1, and V_n may be obtained by taking moments about the line of action at point C_b, as

$$V_n\left(l_v + Z\right) = C_f Z$$

and therefore

$$V_n = 0.85 f_{ck}\beta_1 cb\left(\frac{Z}{l_v + Z}\right) \tag{10}$$

Substituting gives

$$Z = l_e - k_2\left(l_e - c\right) - \beta_1 c/2$$

and

$$\left(l_v + Z\right) = a + l_e - k_2\left(l_e - c\right)$$

Simplifying yields

$$V_n = 0.85 f_{ck}\beta_1 b l_e\left(\frac{c}{l_e}\right)\left[\frac{1 - k_2\left(1 - \frac{c}{l_e}\right) - \frac{\beta_1}{2}\left(\frac{c}{l_e}\right)}{1 - k_2\left(1 - \frac{c}{l_e}\right) + \frac{a}{l_e}}\right] \tag{11}$$

The value of c/l_e was calculated using Equation (9), which corresponded to the values of a/l_e are 0.5 range from to 2.7 for $20.7 < f_{ck}$ /MPa < 55.2, i.e., for β_1 are range from 0.85 to 0.79. Figure 3 shows that the value of c/l_e has only a small variation from its average value. As shown in Fig. 3, the average value of c/l_e is 0.66, and the coefficient of variation was 3.5% for normal-strength concrete. Therefore, the value of c/l_e was assumed to be c/l_e is 0.66. It follows from Equation (11) that k_2 is 0.36. Then, $V_{n(theory)}$ is given by

$$V_{n(theory)} = 0.85 f_{ck}\beta_1 b l_e\left[\frac{0.58 - 0.22\beta_1}{0.88 + a/l_e}\right] \text{ (N)} \tag{12}$$

The flange width was assumed to be fully effective in developing the bearing stresses. Based on these assumptions, and by calibrating using experimental data obtained from steel bracket, precast, corbel, and steel beam-concrete column joint subjected to cyclic loading, the embedment length of the steel coupling beam was computed using Equation (12). The experimental results [10-13] of steel bracket, precast, steel beam-concrete column joint, and coupled shear walls have been used to propose the strength equations of connection between steel coupling beam and reinforced concrete shear wall, as shown in Table 1. Figure 4 shows comparisons between the predicted values from the theoretical equations and the observed strength. As shown in Fig. 4, the predicted values from the theoretical equations underestimate the observed strength.

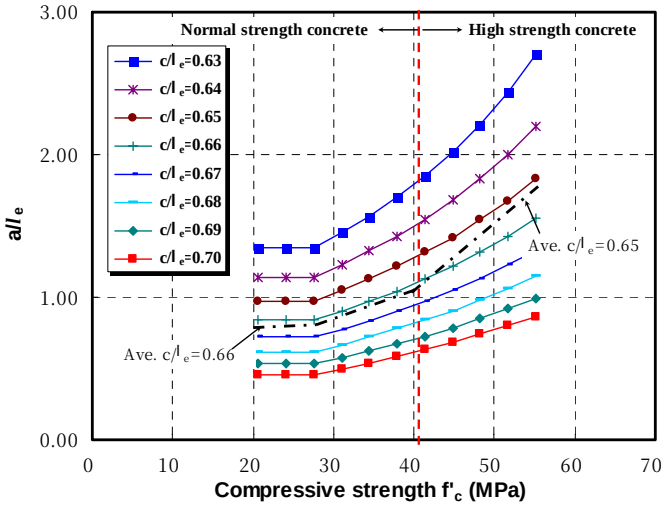

Fig. 3 c/l_e versus concrete compressive strength and a/l_e

2.2 Contributions of auxiliary bars and horizontal ties

Based on the test results from a previous study [16], stud bolts on the top and bottom flange of an embedded steel coupling beam section, as shown in Fig. 2, were specified in an effort to improve the stiffness, and to improve the transfer of the flange bearing force to the surrounding concrete. By taking moments about the line of action, C_b, the additional strength due to the internal moment arm among the stud bolts can be computed using Equation (13)

$$V_s = \frac{2(0.88 - a/l_e)\sum_{i=1}^{n} A_{si} f_{si}}{0.88 + a/l_e} \text{ (N)} \tag{13}$$

A previous study [17] suggests that the longitudinal bars do not typically yield, and hence, the contribution of these bars to joint strength is nominal. Concrete can be confined by horizontal ties, commonly in the form of closely spaced tie reinforcements in the connection region. Horizontal ties through the connection between steel coupling beam and reinforced concrete shear wall result in an increase in the strength and ductility. A previous study by Shahrooz *et al.* [18] pointed to the importance of horizontal ties for enhancing ductility, but did not address the contribution to the bearing strength in the connection.

3. EXPERIMENTAL PROGRAM

Three test specimens were employed, included on wall pier with the other two being steel coupling beams. The test subassemblages were used to review the factors influencing the bearing strength of connection between steel coupling beam and reinforced concrete shear wall. The test variables used are summarized in Table 2. The specimens were cast vertically, but typical construction joints in the

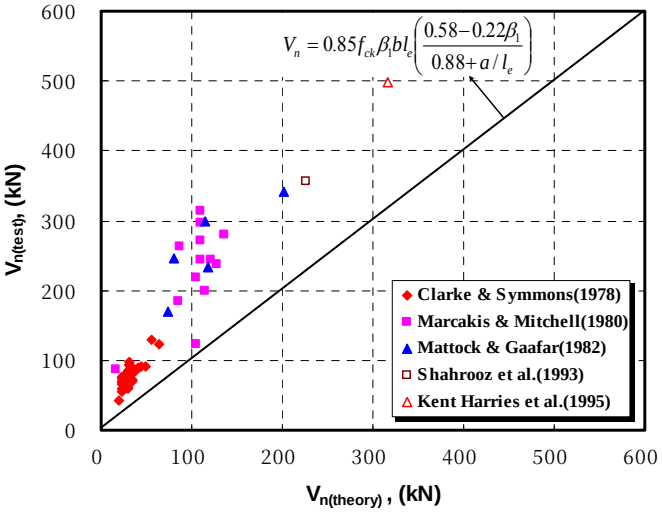

Fig. 4 Comparison of values predicted by theoretical Eq. and observed strength

wall around the connection were not reproduced.

Table 2. Variables of test specimens

Item / Specimens	Stud bolts	Horizontal ties	Wall reinforcements		Eccentricity of vertical load e (mm)
			In wall	In connections	
SCB-ST	None	None	HD13@230	HD13@230	+150
SCB-SB	12-ϕ19	None	HD13@230	HD13@230	+150
SCB-SBVRT	12-ϕ19	4-HD10	HD13@230	HD19@100	+150

Table 3. Average concrete compressive strengths

Item / Specimens	Compressive strength (MPa)	Ultimate strain (μ)	Slump (mm)	Elastic modulus (GPa)	Poisson's ratio
SCB Series	34.0	2,340	145	26,200	0.11

∗ At the time of testing

Table 4. Properties of reinforcement bars and steel

Specimens	Item		Yield strength f_y, (MPa)	Yield strain ε_y, ($\times 10^{-6}$)	Elastic modulus E_s, (GPa)	Ultimate strength f_{su}, (MPa)
SCB Series	Reinforcement	10mm diameter deformed bar	398	2,325	171.2	566
		13mm diameter deformed bar	400	2,533	157.9	555
	Steel	beam web	339	1,682	201.2	461
		beam flange	352	1,827	192.7	489
	Stud bolts	19mm diameter deformed bar	362	1,701	215.8	449

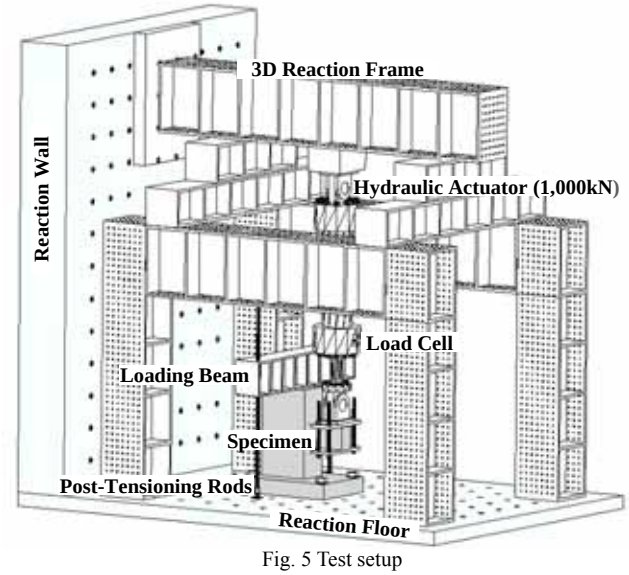

Fig. 5 Test setup

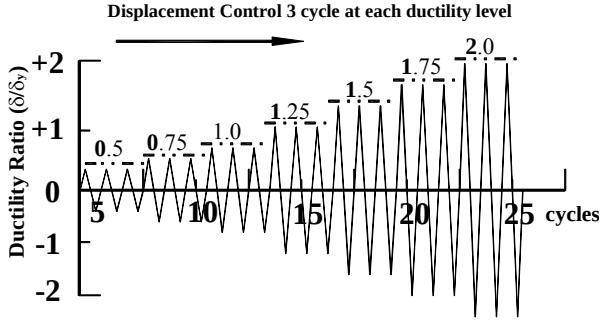

Fig. 6 Loading history

Ready-mix concrete with a minimum specified 28-day compressive strength of 34.0 MPa was used for each of the three specimens. The maximum size of concrete aggregate was 15 mm to ensure good compaction of the concrete in the test specimens. The slump of the concrete was 145mm. For each batch, 100 x 200 mm cylinders were constructed to measure the compressive strength of the concrete. The measured concrete strength and the elastic modulus were tested using the method defined in the ASTM standards.

The horizontal and vertical reinforcement consisted of ϕ=13 mm deformable bars.

The reinforcing steel used for all the walls was obtained from a single batch of steel for each bar diameter, and three specimens were tested from each diameter of reinforcing used. Tension tests were conducted on full-sized bar specimens in accordance with ASTM Standard A370 to determine the yield strength, ultimate strength, and total elongation. The observed material properties are reported in Tables 3 and 4. The data acquisition system used are consisted of 36 internal controls and recording channels. Instrumentation was provided to measure the load, displacement, and strain at critical locations. The displacement of each specimen was measured using Linear Variable Differential Transducers (LVDTs). The vertical displacement profile of each specimen was measured using LVDTs at three locations over the span of the steel coupling beams. A schematic diagram of the test apparatus is shown in Fig. 5. The test specimens were loaded using two hydraulic jacks: a pair of 2,000 kN hydraulic jack for the wall, and a 1,000 kN hydraulic jack for the steel coupling beams. The wall loading is applied with tension rods and hydraulic jack located beneath the reaction floor. The displacement of all the specimens was controlled to follow similar displacement histories with progressively increasing amplitude. The observed displacement history during the tests is shown in Fig. 6; δ_y indicates the yielding displacement of the coupling beams. The data were acquired from the load on the hydraulic jacks, the deflection and rotation of the steel coupling beams, the strain in the longitudinal reinforcing bars and stud bolts in the embedment region, and strain on the flanges and web of the steel coupling beams.

3.1 Experimental results

All the specimens experienced similar damage patterns, consisting of cracking and spalling between the top and bottom flanges, as shown in Fig. 7. For all the specimens, an initial cracking at the steel coupling beam flange-concrete interface was observed during Load stage 1, corresponding to a load of about ± $0.5\delta_y$. On completion of the tests, cracks with a width of up to 3 mm around the top and bottom flanges could be observed. These cracks were approximately 40 mm deep, as shown in Figs. 7(a)–10(c). Finally, spalling of the concrete below the embedded steel coupling beam section began at a load of about 92% of the ultimate load for all the specimens. Figure 7 shows a plot of the applied load versus the steel coupling beam-rotation angle. The bearing strengths of Specimens SCB-ST, SCB-SB, and SCB-SBVRT could develop a bearing force 313,

428.3, and 434 kN, respectively, in the compression cycles (beam push down). In particular, in specimen SCB-ST, the steel coupling beam did not reach the plastic moment capacity, because of wall spalling and bearing failure. As shown in Fig. 7, in specimen SCB-SB, the average strain of the stud bolts on the top and bottom flanges at the ulti-

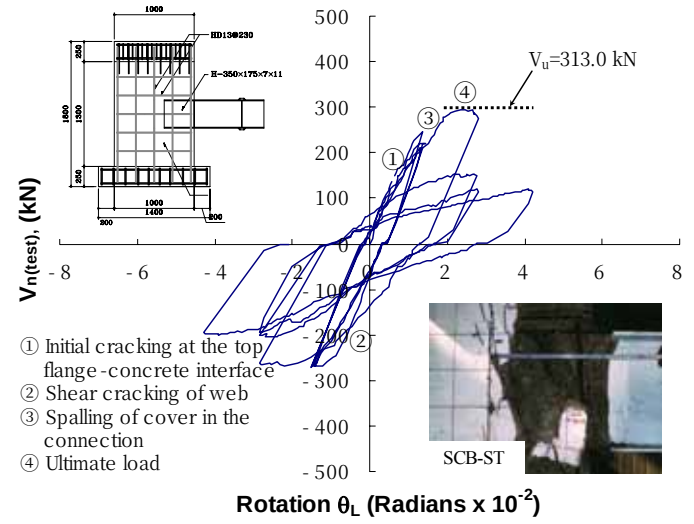

(a) SCB-ST;

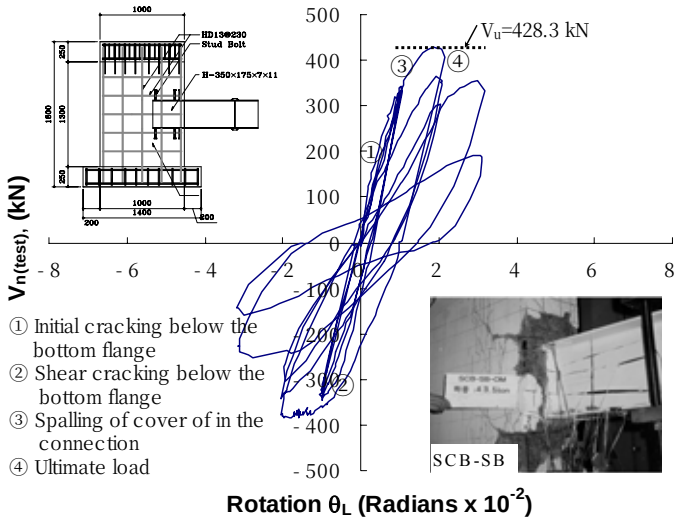

(b) SB; and

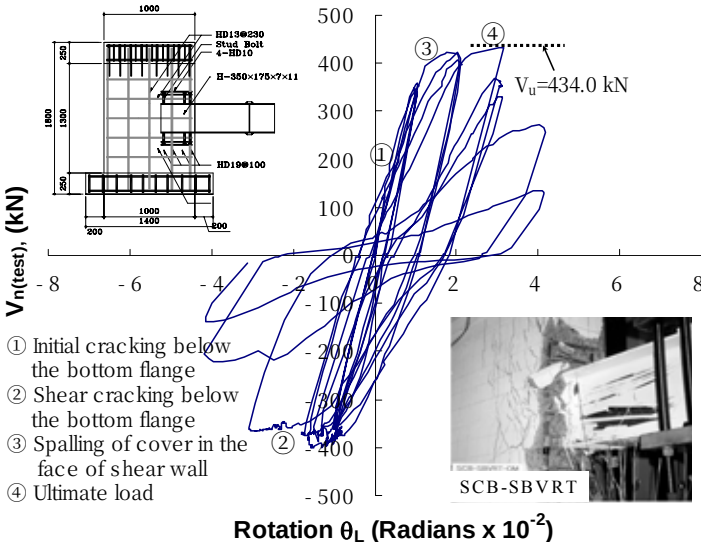

(c) SCB-SBVRT;

Fig. 7 Load versus beam rotation angle hysteretic response

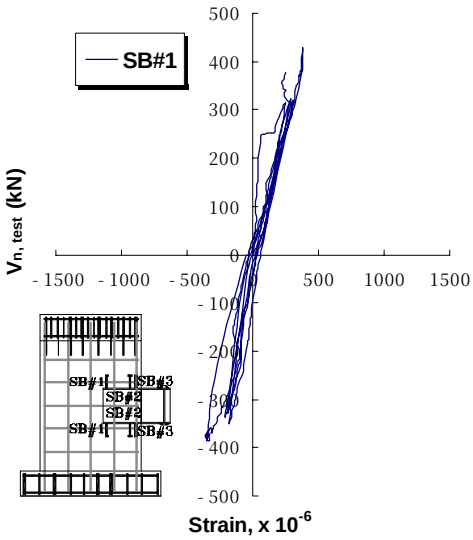

(a) SB#1;

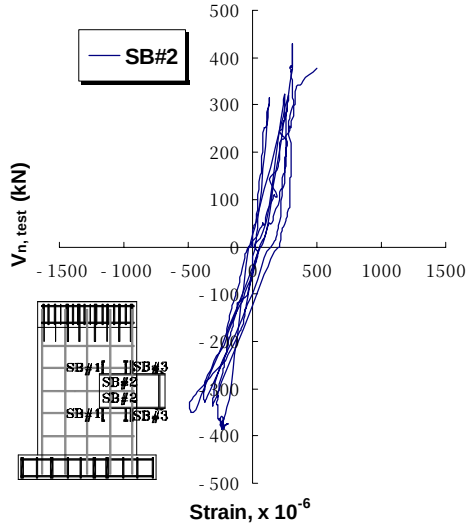

(b) SB#2; and

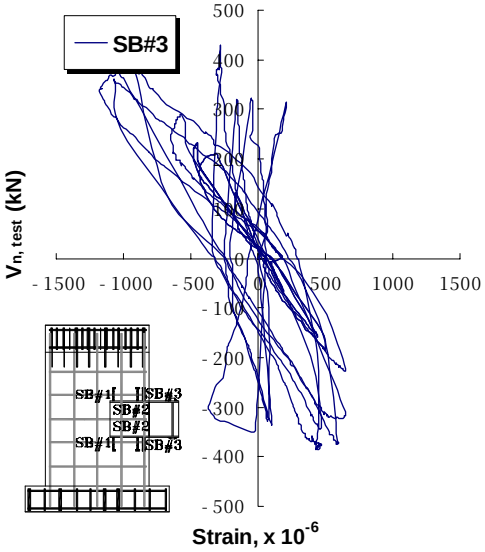

(c) SB#3

Fig. 8 Strain of stud bolts at ultimate load; Specimen SCB-SB

mate load was equal to about 0.000366, 0.000496, and 0.000903 for the three specimens studied. Specimen SCB-SB was reinforced by stud bolts on the top and bottom flanges, and this increased the bearing strength compared with that of specimen SCB-ST by approximately 36.7%.

As shown in Fig. 8, in specimen SCB-SBVRT, the average strain of the horizontal ties on the top and bottom flanges at the ultimate load was equal to about 0.000601, and 0.000550, respectively. The bearing strength of specimen HCWS-SBVRT may be reasonably taken to be about 1.45 and 1.35 times that of specimens HCWS-ST and HCWS-SB, respectively.

3.2 Revision of the influential factors

(1) Bearing stress

The maximum loads carried by the specimens are listed as the values of $V_{n(test)}$ in Table 5. Also listed in this table are the calculated ultimate loads: $V_{n(PCI)}$, using the PCI equation, and $V_{n(theory)}$ using Equation (16) developed in this study. Both equations yield over-conservative estimates of the ultimate strengths of the specimens. The values from the PCI equation are about 40% more conservative than those determined using Equation (16). The degree of conservatism of Equation (16) increases as the width of the embedded steel coupling beam section decreases. This increase in conservatism must be due to an increase in the concrete bearing stress as the ratio of the width of the embedded steel coupling beam, *b*, to the thickness of the shear wall decreases. Similar behavior has been found in tests on column heads subjected to strip loading [4-6].

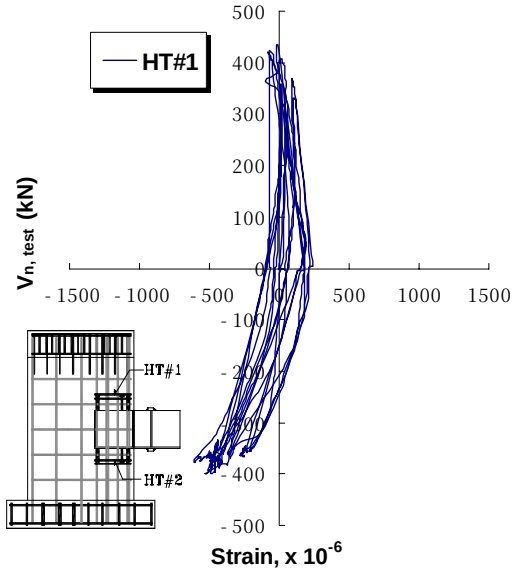

(a) UT1;

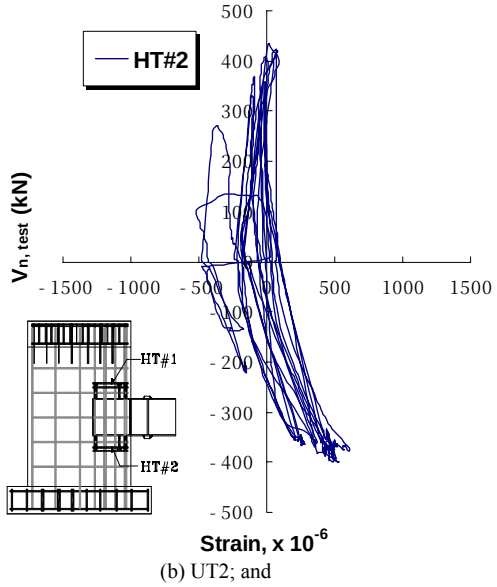

(b) UT2; and

Fig. 9 Strain of horizontal ties at ultimate load; Specimen SCB-SBVRT

The ultimate strength is proportional to the bearing stress, f_b, that was assumed to be equal to $0.85f_{ck}$ when calculating $V_{n(theory)}$. Therefore, we can write

$$V_{n(test)} / f_b = V_{n(theory)} / 0.85 f_{ck} \tag{14}$$

$$f_b / f_{ck} = 0.85 V_{n(test)} / V_{n(theory)} \tag{15}$$

The values of f_b/f_{ck} calculated using Equation (15) are given in Table 5. The values of f_b/f_{ck} for specimens SCB-ST, SCB-SB, SCB-SBVRT, and other test data (for which the bearing width, b, is the width of the steel coupling beams) are plotted against the ratio of b over t in Fig. 10, where t is the thickness of the shear walls (or width of column). A point corresponding to the case where f_b/f_{ck} is equal to 0.85 when *b* over *t* is unity is also plotted, *i.e.*, a bearing on the full thickness of the shear walls. For a member without any horizontal ties, it can be seen that the variation of f_b/f_{ck} with *b* over *t* can be represented closely by

$$f_b / f_{ck} = 0.85\left(\frac{b}{t}\right)^{-0.55} \tag{16}$$

or

$$f_b = 28.9\left(\frac{b}{t}\right)^{-0.55} \quad \text{(MPa)} \tag{17}$$

For a member with horizontal ties

$$f_b / f_{ck} = 0.85\left(\frac{b}{t}\right)^{-0.60} \tag{18}$$

or

$$f_b = 28.9\left(\frac{b}{t}\right)^{-0.60} \quad \text{(MPa)} \tag{19}$$

for this group of specimens with an average value of f_{ck} is 34.0 MPa.

Table 5. Test results

Specimens	a (mm)	l_e (mm)	f_{ck} (MPa)	$V_{n(test)}$ (kN)	$V_{n(PCI)}$ (kN)	$\frac{V_{n(test)}}{V_{n(PCI)}}$	$V_{n(theory)}$ (kN)	$\frac{V_{n(test)}}{V_{n(theory)}}$	$\frac{f_b}{f_{ck}}$	Failure mode
SCB-ST	600	374	34.0	313.0	190.9	1.64	258.9	1.21	1.03	Bearing failure
SCB-SB	600	374	34.0	428.3	256.9	1.66	258.9	1.65	1.41	Bearing failure
SCB-SBVRT	600	374	34.0	434.0	256.9	1.69	258.9	1.50	1.42	Bearing failure

1mm=0.03937in.
1MPa=145.14psi.
1kN=0.2248kip.

(2) Tensile stress

The studies in References [7] and [8] found that the concrete bearing strength under strip loading was proportional to the concrete tensile strength, f_{sp}, rather than to the compressive strength, f_{ck}. The authors of References 7 and 8 assumed that f_{sp} was proportional to $\sqrt{f_{ck}}$ and proposed equations of the following form, as shown in Fig. 11

$$f_b = A\sqrt{f_{ck}}\left(\frac{t/2}{b}\right)^n \quad \text{(MPa)} \qquad (20)$$

$$f_b = K\sqrt{f_{ck}}\left(\frac{t}{b}\right)^n \quad \text{(MPa)} \qquad (21)$$

where b is the width of the steel coupling beam.

Kriz and Raths [7] proposed values of A is 5.7 and n is 0.33, *i.e.*, K corresponding to $A/2^n$ is 4.5, and Hawkins [19-21] suggested that for design purposes, the values of A and n proposed by Kriz and Raths [7]should be used. Williams proposed a value of n = 0.47. In view of the findings shown in References [7] and [8], we proposed that the bearing stress below embedded sections at ultimate load be expressed in the same form as Equation (21).

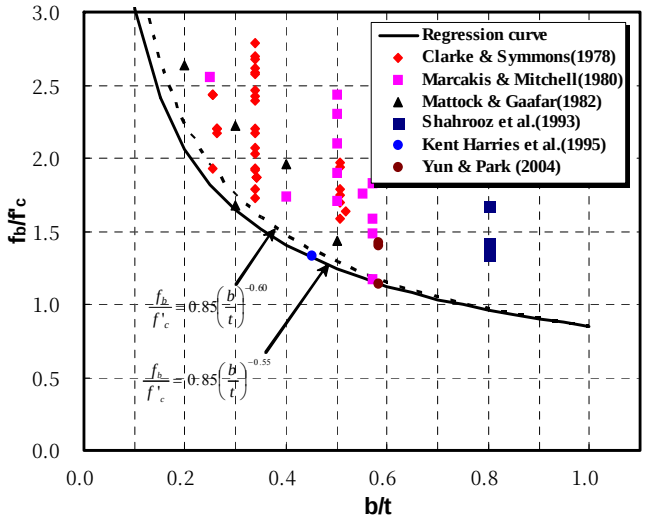

Fig. 10 Variation of bearing stress at ultimate load with ratio b/t

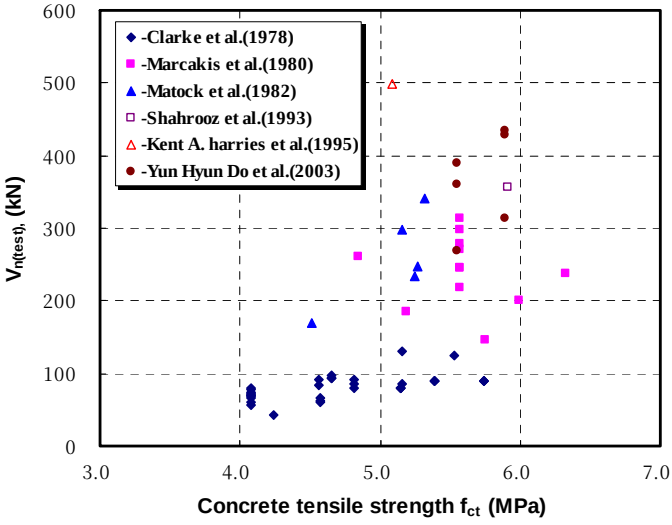

Fig. 11 Revision of influential factors

For member without horizontal ties, by comparing Equations (17) and (21), n is 0.55 and $K\sqrt{f_{ck}}$ is 28.9 MPa when f_{ck} is 34.0 MPa. Hence, the value of K is 4.9, which is very close to the value of A determined by Kriz and Raths [7]. Substituting the value of K is 4.5 proposed by Kriz and Raths [7] into Equation (21), the bearing strength of concrete for an embedded steel coupling beam section without horizontal ties can be calculated using

$$V_{n(revised)} = f_b \beta_1 b l_e \left(\frac{0.58 - 0.22\beta_1}{0.88 + a/l_e}\right) \quad \text{(N)} \qquad (22)$$

$$f_b = 4.5\sqrt{f_{ck}}\left(\frac{t}{b}\right)^{0.55} \quad \text{(MPa)} \qquad (23)$$

The value of n corresponding to 0.66 proposed by Mattock and Gaafar is somewhat higher than the values for n proposed in this study. This may be the result of additional lateral confinement of the loaded area below an embedded steel coupling beam section, resulting from a continuity of the concrete around the embedded steel coupling beam section, and from the presence of closely spaced tie reinforcements in the column. Therefore, for a member with minimal horizontal ties

$$f_b = 4.5\sqrt{f_{ck}}\left(\frac{t}{b}\right)^{0.60} \quad \text{(MPa)} \qquad (24)$$

Until further test data are available, it is proposed that value of the ratio of t/b not be t/b > 2.2 when using Equations (23) and (24).

4. PROPOSAL OF STRENGTH EQUATION

As governed by the bearings on the concrete, we proposed that the bearing strength of connection between steel coupling beam and reinforced concrete shear wall can be calculated using the following equation

$$V_{n(proposed)} = f_b \beta_1 b l_e \left(\frac{0.58 - 0.22\beta_1}{0.88 + a/l_e}\right) + \frac{2(0.88 - a/l_e)\sum_{i=1}^{n} A_{si} f_{si}}{0.88 + a/l_e} \quad \text{(N)} \qquad (25)$$

For a member without horizontal ties

$$f_b = 4.5\sqrt{f_{ck}}\left(\frac{t}{b}\right)^{0.55} \quad \text{(MPa)} \qquad (26)$$

and for a member with horizontal ties

$$f_b = 4.5\sqrt{f_{ck}}\left(\frac{t}{b}\right)^{0.60} \quad \text{(MPa)} \qquad (27)$$

where β_1 is ratio of the depth equivalent rectangular stress distribution to the depth of flexural compression zone as specified in Section 10.2.7 of ACI 318-02, A_{si} is cross-sectional area of the auxiliary bar, *i*, inside the joint, and f_{si} is stud stresses in the auxiliary bar, *i*, inside the joint.

5. EXPERIMENTAL VERIFICATION

Additional experiments were conducted to verify the

strength equation for the connection between steel coupling beam and reinforced concrete shear wall. The test variables of the HCWS series specimens were identical to those of the SCB series specimens, except that the concrete compressive strength, f_{cu}, was 30.0 MPa, as listed in Table 6. Table 7 shows the test results of the HCWS series specimen to verify the strength equation and for comparison with the results from the SCB series specimens that were conducted previously.

5.1 Crack and damage pattern

Figure 12 shows the failure modes for the connection between steel coupling beam and reinforced concrete shear wall tested. Stress in the embedment region caused by reversed cyclic loading resulted in an alternating compression zone in the concrete at the top and bottom flanges of the steel coupling beam near the face of the shear wall. In specimen HCWS-ST, initial cracking at the steel coupling beam flange-concrete interface was observed at Load stage 1, corresponding to a load of about $\pm$ 0.5δ_y. Horizontal cracks located at the flange-concrete interface extended from the flange across the inner face of the wall to the side faces of the wall, as shown in Fig. 12(a). Localized spalling and crushing of the concrete along the top and bottom flanges of the coupling beam, at the front of the compression zone, was initially observed at a displacement ductility level of 1.75.

Table 6. Average concrete compressive strengths

Item / Specimens	Compressive strength f_{cu}, (MPa)	Ultimate strain (μ)	Slump (mm)	Elastic modulus E_c, (MPa)	Poisson's Ratio ν
HCWS Series	30.0	2,484	150	25,900	0.11

Table 7. Correlation of test and predicted strengths

Specimen	SCB-ST	SCB-SB	SCB-SBVRT	HCWS-ST	HCWS - SB	HCWS - SBVRT
Failure mode	Bearing failure	Bearing failure	Bearing failure	Bearing failure	Bearing failure	Bearing failure
$V_{n(test)}$, (kN)	313.0	428.3	434.0	268.2	361.2	390.3
$V_{n(PCI)}$, (kN)	190.9	256.9	256.9	152.7	226.7	226.7
$V_{n(Kriz\ \&Rath)}$, (kN)	280.2	280.2	280.2	238.2	238.2	238.2
$V_{n(Willaims)}$, (kN)	274.2	274.2	274.2	233.1	233.1	233.1
$V_{n(Mattock)}$, (kN)	354.8	354.8	354.8	301.6	301.6	301.6
$V_{n(theory)}$, (kN)	258.9	258.9	258.9	207.4	207.4	207.4
$V_{n(proposed)}$, (kN)	313.0	424.6	433.1	261.2	354.0	361.1
$\frac{V_{n(test)}}{V_{n(PCI)}}$	1.64	1.66	1.69	1.76	1.59	1.72
$\frac{V_{n(test)}}{V_{n(Kriz\ Rath)}}$	1.12	1.53	1.39	1.13	1.52	1.64
$\frac{V_{n(test)}}{V_{n(Willials)}}$	1.14	1.56	1.42	1.15	1.55	1.67
$\frac{V_{n(test)}}{V_{n(Mattock)}}$	0.88	1.22	1.09	0.89	1.20	1.29
$\frac{V_{n(test)}}{V_{n(theory)}}$	1.21	1.65	1.50	1.29	1.74	1.88
$\frac{V_{n(test)}}{V_{n(proposed)}}$	1.00	1.01	1.00	1.00	1.02	1.08

However, the stud bolts of specimens HCWS-SB and HCWS-SBVRT were an effective means of controlling the gap opening occurring between the steel coupling beam flange and the concrete interface at low load levels, as shown in Figs. 12(b) and 15(c). The spalling of the embedment region near the inner face of the wall extended a distance of about 200 mm into the wall in the final stages of the tests, resulting in exposure of the first set of vertical reinforcing bars.

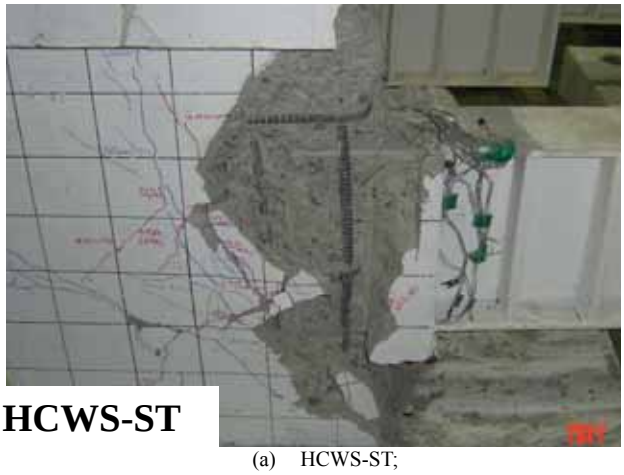

(a) HCWS-ST;

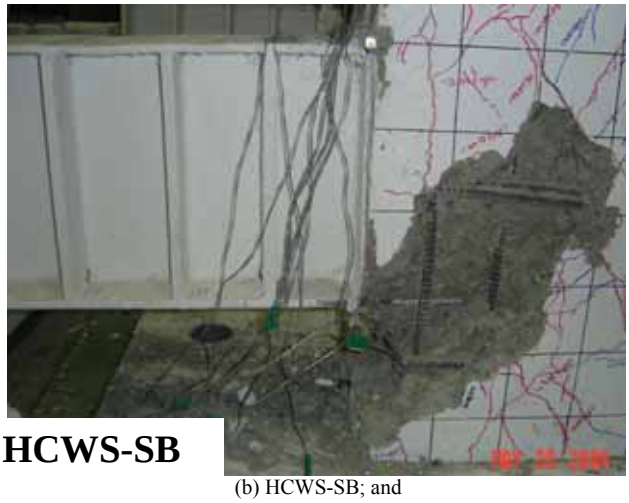

(b) HCWS-SB; and

(c) HCWS-SBVRT

Fig. 12 Cracking pattern

5.2 Hysteretic response

A graph of the applied load versus the steel coupling beam-rotation angle is shown in Fig. 13. All three specimens did not exhibit any stable spindle-type hysteretic loops. However, the stiffness characteristics were different

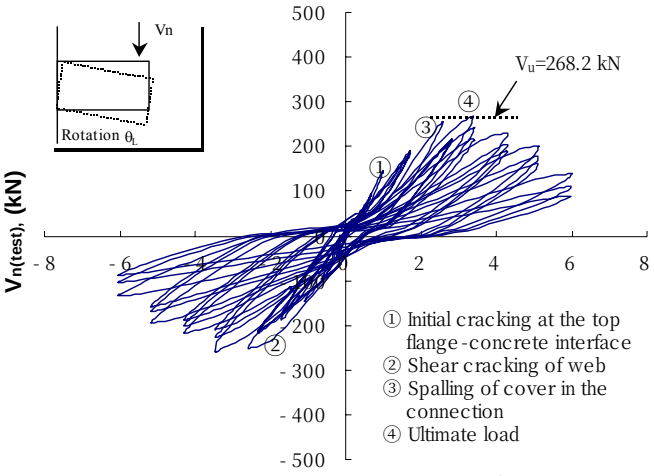

(a) HCWS-ST;

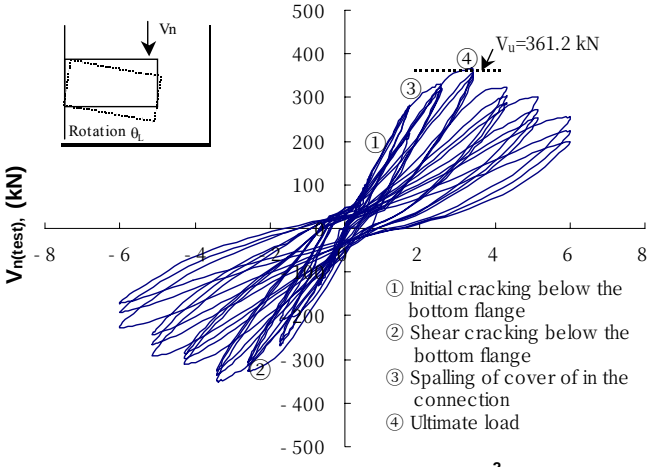

(b) HCWS-SB; and

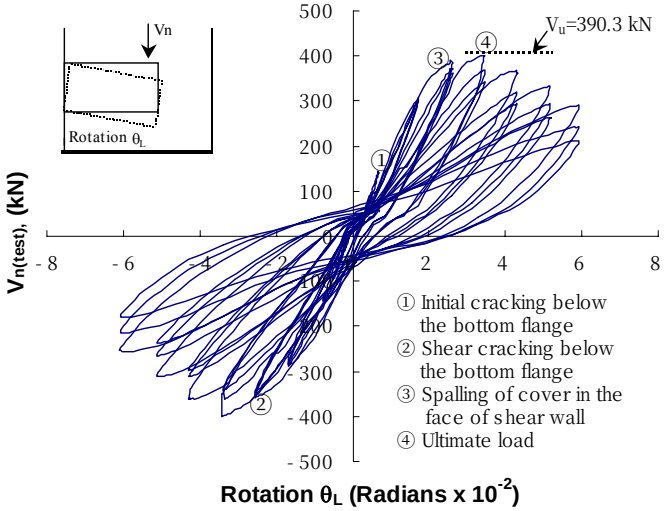

(c) HCWS-SBT

Fig. 13 Load versus beam rotation angle hysteretic response

for the compression and tension cycles. For the compression cycles, the boundary element was subject to compressive stresses, which led to an improved transfer of forces from the coupling beam into the wall. Under tension cycles (*i.e.*, when the beam was pulled up), the boundary element was subjected to tensile stresses. The tensile stresses resulted in cracking, and a reduced degree of fixedness of the coupling beam in the wall was observed. As shown in Fig. 13(a), specimen HCWS-ST showed a sudden decrease in strength during the first and second cycles at a displacement ductility level corresponding to 1.5. Compared with specimen HCWS-ST, specimens HCWS-SB and HCWS-SBVRT showed stable repeatability through each cycle for each displacement level after the maximum strength had been achieved, as shown in Figs. 13(b) and 16(c). These can be attributed to the effect of the stud bolts and the confinement of the surrounding concrete by the horizontal ties.

As listed in Table 7, specimens HCWS-ST, HCWS-SB, and HCWS-SBVRT could be subjected to a bearing force 268.2, 361.2, and 390.3 kN, respectively, in the compression cycles (beam pushed down). The bearing strength of specimen HCWS-SBVRT may be reasonably taken as being about 1.46 and 1.08 times that of specimens HCWS-ST and HCWS-SB, respectively. The stud bolts and horizontal ties on the top and bottom of the steel coupling beam flanges in the connection region can efficiently resist high bearing stresses.

5.3 Stiffness characteristics

The variation in the secant stiffness, *i.e.*, the ratio between the maximum strength and the maximum rotation angle of the steel coupling beam at each stage, V_{max}/θ_L with respect to the beam rotation angle, is compared in Fig. 14. To assess the rate of stiffness degradation of the steel coupling beams, ratios of the stiffness at each stage to the initial stiffness of all the specimens were obtained. The stiffness degradation was computed from the change in stiffness with rotation angle.

In Fig. 14, the initial stiffness of all the specimens had similar values within the range from 60.12 to 63.75 kN/mm, but with increasing rotation angle, the stiffness degradation became significant with changes in rotation angle. For the rotation angle of θ corresponding to 0.052 rad, the stiffness degradation ratios of specimens HCWS-ST, HCWS-SB, and HCWS-SBVRT were 62.7, 51.8, and 49.6%, respectively. Therefore, the reinforcing details of the connection influenced the stiffness degradation value.

5.4 Energy dissipation characteristics

The energy dissipation characteristics of a member are an important measure of its seismic performance. The hysteretic response of steel coupling beams arise from a combination of yield of the steel coupling beam outside of the shear wall and the plasticity of the connection region, *i.e.*, the yielding of the beam in the embedded region and the fracture of the surrounding concrete. An effective design requires that the latter characteristic be small in relation to

the former characteristics. In the tests, as the response of the walls remained approximately in the elastic range, the participation of the wall segment towards the total dissipated energy was deemed insignificant.

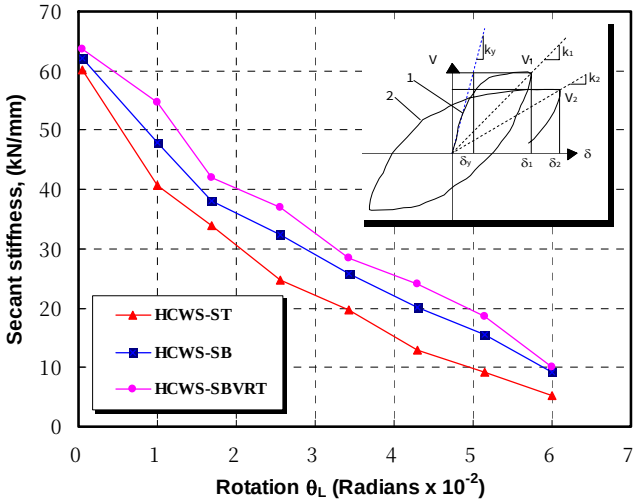

Fig. 14 Secant stiffness degradation

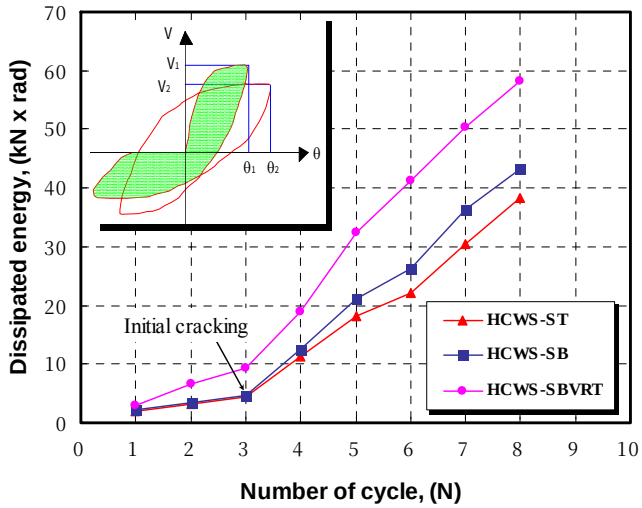

Fig. 15 Cumulative dissipated energy

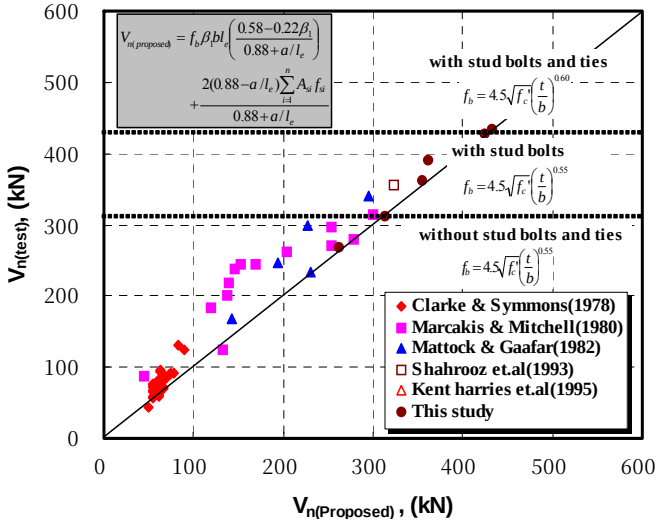

Fig. 16 Comparison of predicted values by proposed equation and observed strength

A graph of the cumulative dissipated energy versus number of cycles is plotted in Fig. 15, showing that the total energy of specimens HCWS-ST, HCWS-SB, and HCWS-SBVRT during the test to 85% conventional failure level was 38.4, 43.2, and 58.1 kN-rad., respectively. It was found that, compared with the other reinforcement details, the stud bolts and horizontal ties were highly effective in increasing the energy dissipation capacity of connection between steel coupling beam and reinforced concrete shear wall.

5.5 Assessment of the proposed equation

Figure 16 shows a comparison of the experimental and predicted data from the proposed equations for the connection between steel coupling beam and reinforced concrete shear wall. When Equation (25) was used to calculate the bearing strength of the specimens tested in this study, then the average values of the ratio of $V_{n(test)}/V_{n(proposed)}$ for specimens HCWS-ST, HCWS-SB, and HCWS-SBVRT of 1.00, 1.02 and 1.08, respectively, were obtained, with standard deviations of 0.15, 0.12, and 0.17, respectively. As shown in Fig. 16, the predicted values from the proposed equations are in good agreement with the measured strengths.

6. CONCLUSIONS

The following conclusions were derived from the results of the experiments and analytical work carried out in this study on the bearing strength of connection between steel coupling beam and reinforced concrete shear wall:

1. In extracting the theoretical Equation (11) for the bearing strength of connection between steel coupling beam and reinforced concrete shear wall, the assumption of a constant value of $c/l_e = 0.66$ is reasonable.
2. The length of the concrete compression zone below the embedded steel coupling beam is effectively constant, and is equal to about 72% of the embedded length of the steel coupling beam.
3. The concrete bearing stress below the embedded steel coupling beams section decreases significantly as the ratio of the width of the steel coupling beam to the width of the shear wall increases. This trend is similar to, but less marked than, the trend observed for bracket, corbel, and beam-column joint.
4. The bearing strength of specimens HCWS-SBVRT and HCWS-SB may be reasonably taken to be about 1.45 and 1.35 times that of specimen HCWS-ST, respectively. Therefore, stud bolts and horizontal ties on the top and bottom of the steel coupling beam flanges in the connection region can efficiently resist high bearing stress.
5. When calculating the bearing strength of a steel coupling beam section embedded in a shear wall, the PCI Code and other proposed models yield very conservative results. Therefore, from this study, the following equations are proposed to calculate the bearing strength of the connection between steel coupling beam and reinforced concrete shear wall

$$V_{n(proposed)} = f_b \beta_1 b l_e \left(\frac{0.58 - 0.22\beta_1}{0.88 + a/l_e} \right) + \frac{2(0.88 - a/l_e)\sum_{i=1}^{n} A_{si} f_{si}}{0.88 + a/l_e} \quad \text{(N)}$$

For a member without horizontal ties

$$f_b = 4.5\sqrt{f_{ck}} \left(\frac{t}{b} \right)^{0.55} \quad \text{(MPa)}$$

and for a member with horizontal ties

$$f_b = 4.5\sqrt{f_{ck}} \left(\frac{t}{b} \right)^{0.60} \quad \text{(MPa)}$$

REFERENCES

1. Pauley, T., and Binney, J. R., "Diagonally Reinforced Coupling Beams of Shear Walls." Shear in Reinforced Concrete: Publication No. 42, Amer. Concrete Inst., Detroit, USA, 1974, pp. 579–598.
2. Shiu, K. N., Barney, G. B., Fiorato, A. E., and Corley, W. G., "Reversed Load Tests of Reinforced Concrete Coupling Beams." Proceedings of the Central American Conf. on Earthquake Engineering, El Salvador, 1978, pp. 239–249.
3. Roeder, C. W., and Popov, E. P., "Eccentrically Braced Steel Frames for Earthquakes." J. Struct. Div., ASCE, 104(3), 1978, pp. 391–411.
4. Gong, B., and Shahrooz B. M., "Concrete-Steel Composite Coupling Beams" Journal of the Structural Division, ASCE, Vol. 127, No. 6, 2001, pp. 625–631.
5. VPCI Manual on Design of Connections for Precast Prestressed Concrete, Prestressed Concrete Institute, Chicago, 1973, pp. 25–38.
6. PCI Design Handbook – Precast and Prestressed Concrete, Prestressed Concrete Institute, Chicago, 1978, pp. 370.
7. Kriz, L. B., and Raths, C. H., "Connection in Precast Concrete Structures – Shear strength of Column Heads," Journal, Prestressed Concrete Institute, V. 8, No. 6, Dec. 1963, pp. 45–75.
8. Williams, A., "The Bearing Capacity of Concrete Loaded Over a Limited Area," Technical Report No. 526, Cement and Concrete Association, London, Aug. 1979, pp. 70–80
9. Mattock, A. H, and Gaafar, G. H., "Strength of Embedded Steel Sections as Brackets," ACI Journal, V. 79-9, March-April, 1982, pp. 83–93.
10. Clarke, J. L., and Symmons, R. M., "Test on Embedded Steel Billets for Precast Concrete Beam Column Connection," Technical Report No. 42. 523, Cement and Concrete Association, London, Aug. 1978, pp. 12–24.
11. Marcakis K, and Mitchell D, "Precast Concrete Connection with Embedded Steel Member," Journal, Prestressed Concrete Institute, V. 25, No. 4, July-Aug. 1980. pp. 86–116.
12. Shahrooz B. M., Remmetter M. A., Qin F., "Seismic Design and Performance of Composite Coupled Walls," Journal of the Structural Division, ASCE, Vol. 119, No. 11, 1993, pp. 3291–3309.
13. Harries, K. A., "Seismic Design and Retrofit of Coupled Walls using Structural Steel," Department of Civil and Applied Mechanics, McGill University, Montreal, Canada, 1995.
14. ACI Committee 318, "Building Code Requirements for Structural Concrete and Commentary," American Concrete Institute, Detroit, USA 2002, pp. 105–110.
15. Kent, D. C and Park, R., "Flexural Members with Confined Concrete," Journal of the Structural Division, ASCE, Vol. 97, ST7, July 1971, pp. 1969–1990.
16. Gong B., and Shahrooz B. M., Gillum A. J., "Cyclic Response of Composite Coupling Beams," ACI Committee 335 Special Publication, 1997.
17. Gong B., and Shahrooz B. M., "Concrete – Steel Composite Coupling Beams," Journal of Structural Engineering, V. 127, No. 6, June, 2001, pp. 625–631.
18. Shahrooz B. M., Remmetter M. A., Qin F., "Seismic Response of Composite Coupled Walls," Composite Construction in Steel and Concrete II, ASCE, New York, N. Y., 1992, pp. 428–441.
19. Hawkins, N. M., "The Shear strength of Concrete for Strip Loading," Magazine of Concrete Research (London), V. 22, No. 71, June 1970, Aug. 1979, pp. 87–97.
20. Park, W. S., and Yun, H. D., "Seismic Behaviour of Steel Coupling Beams Linking Reinforced Concrete Shear Walls," Engineering Structure, In press
21. Park, W. S., Yun, H. D., Hwang. S. K., Han, B. C., and Yang, I. S., "Shear Strength of the Connection between a Steel Coupling Beams and a Reinforced Concrete Shear Walls in a Hybrid Wall System," Journal of Constructional Steel Research, V. 61, No. 7, pp. 912-941.

NOTATION

a	= distance from the concentrated load to the face of the column or shear wall (in mm)
A	= coefficient in Equation (15).
b	= width of the embedded steel section (in mm).
b_{eff}	= effective width of the concrete compression block (in mm).
c	= length of compression zone below embedded steel section (in mm).
C_b	= resultant concrete compressive force acting on top and at back of embedded steel section (in N).
C_f	= resultant concrete compressive force acting below and at front of embedded steel section (in N).
e	= lever arm of load applied to embedment (in mm).
f_b	= concrete bearing stress (in MPa).
f_c	= concrete stress (in MPa).
f_{cu}	= concrete compressive strength measured on 150×300 mm (6×12 in.) cylinders (in MPa).
l	= clear span of coupling beam (in mm).
l_e	= length of the embedment of steel coupling beam in concrete shear wall (in mm).
l_{eff}	= effective clear span of the coupling beam (in mm).
l_v	= distance from concentrated load to the resultant compression force C_f (in mm).
n	= exponent in Equations (15) and (16).
t	= width of column or thickness of the shear wall (in mm).
V	= concentrated load acting on the embedded section (in N).
V_n	= nominal strength, i.e., value of load V at ultimate strain (ϕ=1.0) (in N).
β_1	= ratio of the depth equivalent rectangular stress distribution to the depth of flexural compression zone as specified in Section 10.2.7 of ACI 318-02.
ε	= concrete strain.
ε_b	= strain in the concrete above the rear end of the embedded steel section.

(Data of Submission : 2005. 1.4)